

Total System Energy Minimization for Wireless Image Transmission

Swaroop Appadwedula, Manish Goel, Naresh R. Shanbhag,
Douglas L. Jones, and Kannan Ramchandran[†]

Department of Electrical and Computer Engineering
Coordinated Science Laboratory
University of Illinois at Urbana-Champaign
1308 W. Main Street, Urbana, IL 61801
email: {appadwed, m-goel1, shanbhag, dl-jones}@uiuc.edu

[†] Department of Electrical Engineering and Computer Science
University of California
269 Cory Hall, Berkeley, CA 94720
email: kannanr@eecs.berkeley.edu

Abstract

In this paper, we focus on the total-system-energy minimization of a wireless image transmission system including both digital and analog components. Traditionally, digital power consumption has been ignored in system design, since transmit power has been the most significant component. However, as we move to an era of pico-cell environments and as more complex signal processing algorithms are being used at higher data rates, the digital power consumption of these systems becomes an issue. We present an energy-optimized image transmission system for indoor wireless applications which exploits the variabilities in the image data and the wireless multipath channel by employing dynamic algorithm transformations and joint source-channel coding. The variability in the image data is characterized by the rate-distortion curve, and the variability in the channel characteristics is characterized by the path-loss and impulse response of the channel. The system hardware configuration space is characterized by the error-correction capability of the channel encoder/decoder, number of powered-up fingers in the RAKE receiver, and transmit power of the power amplifier. An optimization algorithm is utilized to obtain energy-optimal configurations subject to end-to-end performance constraints. The proposed design is tested over QCIF images, IMT-2000 channels and $0.18\mu m$, $2.5V$ CMOS technology parameters. Simulation results over various images, various distances, two different channels, and two different rates show that the average energy savings in utilizing a total-system-energy minimization over a fixed system (designed for the worst image, the worst channel and the maximum distance) are 53.6% and 67.3%, respectively, for short-range (under $20m$) and long-range (over $20m$) systems.

*This research was supported by the NSF award MIP-9707742 and NSF CAREER award MIP-9623737.

1 Introduction

There is widespread use of portable wireless technology in the form of cellular phones, wireless networks, wireless surveillance systems and other wireless devices. In order to avoid frequent recharging and possible down-time, the power consumption of these systems must be minimized. Currently, most low-power wireless systems are designed by minimizing the transmit power, since it is usually the most significant component of the total system power consumption. In addition to hardware design techniques, powerful channel-coding algorithms provide coding gain and significantly reduce transmit power. Complex source coding algorithms provide the reduction in data rates necessary for efficient use of bandwidth. Traditionally, the power consumption due to these complex signal processing algorithms has been considered negligible. However, as we move towards an era of micro-cells and pico-cells, the power consumption of the baseband processing unit becomes comparable to that of the power amplifier. Efforts such as Bluetooth [1] for short-range radio links in portable devices such as mobile PCs and mobile phones, as well as the HomeRF [2] open industry specification for RF digital communications in the home, are some examples of steps toward pico-cell communications. Therefore, techniques which jointly minimize the power consumption in the power amplifier and the baseband processing unit are desirable.

Increasing the complexity of the channel coding algorithm to increase coding gain and lower transmit power increases the baseband processing power. Similarly, at short distances, using a less complex source coder which keeps some redundancy in the encoded stream may allow us to use a less complex channel coder, thereby providing more energy for the power amplifier. In [3], Lan and Tewfik found that, for low transmission power, a less efficient source coder, which consumes less power and achieves less compression, combined with a channel coder that adds very little redundancy, is energy-optimal. Therefore, the task of minimizing the baseband processing power and minimizing the power amplifier power are inseparable.

The joint minimization of the total system power is subject to the system resource constraint of bandwidth and the performance constraint of end-to-end image quality. For source image data requiring a high rate to achieve a desired image quality, the channel coder can only introduce a small amount of redundancy due to the bandwidth constraint, and more power may be drawn by the power amplifier. There are operating conditions for which coding gain is more important than

transmit power, and other operating conditions for which leaving the redundancy in the source consumes less power than adding redundancy in the channel coder. An adaptive technique which chooses the optimal system configuration based on the input and channel condition is necessary to achieve maximum performance in all regimes.

In this work, we focus on the design of a reconfigurable wireless image transmission system that achieves low power by exploiting both the variabilities in the image data and the multipath wireless channel. Reconfigurable digital signal processing (RDSP) [4] has been proposed as a low-power technique that exploits variabilities in the environment. Energy savings are achieved by tailoring the architecture to the environment. In [5]- [6], *dynamic algorithm transforms (DAT)* were proposed as a systematic framework for designing low-power reconfigurable signal processing systems. DAT requires the definition of: (1) input state-space, (2) configuration-space, (3) energy models and (4) DSP algorithm performance models. The input state-space models the input variabilities, and the configuration-space is the set of possible hardware configurations. Energy models and performance models are employed to obtain estimates of the energy consumption and a performance metric (such as distortion or bit-error rate).

In order to exploit the relationship between the configuration space, the input space and the DSP algorithm performance metric, we employ recent advances in joint source-channel coding (JSCC) [7] and DAT [6]. Significant past work on joint source-channel coding has shown that the tradeoff between data and redundancy can be exploited to design optimal realizable systems [8], [9], [10]. The application of joint source-channel coding in heterogeneous, multi-media environments leads to general matching techniques, which have been the focus of some current research [7], [11], [12]. In [7], we developed a general matching technique which can be applied to a wide variety of source coders and channel coders. These methods maximize the end-to-end quality of a transmitted image subject to constraints on the transmit power and bandwidth. In this work, we combine these methods with techniques for RDSP to jointly optimize the baseband processing power and the transmit power of a reconfigurable system.

The proposed system can be motivated as follows. In Figure 1(a), we have plotted the rate-distortion curves for different images encoded via a *set partitioning in hierarchical trees (SPIHT)* [13] encoder, which is a state-of-the-art compression scheme. It can be seen that the encoder needs to operate at different rates to obtain a specified distortion (in terms of peak signal-to-noise-ratio

PSNR) of $35dB$. Similarly, channel variabilities are characterized by different values of E_b/N_0 (where E_b is the energy per bit and N_0 is the noise power spectral density) in Figure 1(b). Each curve in Figure 1(b) corresponds to a different number of correctable errors, t , for a Reed-Solomon code. It can be seen that the channel encoder needs to operate at a different t (for different E_b/N_0) to meet a specified bit-error rate (BER) constraint of 10^{-3} . Thus, if the image changes from “*coastguard*” to “*carphone*” and the channel E_b/N_0 changes from $5dB$ to $7dB$, then to keep the PSNR the same, one must adjust the source rate, the number of correctable errors, the transmit power, and the number of RAKE fingers (in case of multipath channels). There are numerous choices for these parameters that can meet the end-to-end distortion constraint. The optimal parameters which minimize the total power consumption are obtained via joint source-channel coding techniques and dynamic algorithm transforms developed in this paper.

In this paper, we develop a technique for optimizing power consumption in flexible systems with performance constraints and time-varying inputs. We apply our energy minimization technique to image transmission over an indoor wireless link to demonstrate the power savings due to our approach. The optimization problem is formulated in terms of the system parameters and includes the reconfigurable blocks. For the image transmission example, the source codec, channel codec, RAKE receiver and power amplifier are the potentially reconfigurable blocks. Energy consumption is minimized by solving an optimization problem which has energy per pixel as the objective function and constraints on the desired distortion and maximum available bandwidth. The proposed reconfigurable system is tested via the evaluation methodology in [14].

The rest of the paper is organized as follows. In the next section, we present an overview of the system. In section 3, we present the optimization for determining the optimal configuration parameters. In section 4, we present the key ingredients such as energy and performance models. The simulation setup and results are presented in section 5.

2 Wireless Image Transmission System

We consider the indoor wireless communication system shown in Figure 2 in which two terminals communicate with each other. Using DAT and JSCC methods, we formulate the problem of efficient image transmission subject to an end-to-end performance requirement. We define (a) an input state space \mathcal{S} , (b) a configuration space \mathcal{C} , (c) models for the DSP algorithms in order to

estimate distortion \mathcal{D} , and (d) energy models for estimating energy consumption \mathcal{E} .

We also make a few assumptions regarding the problem which make our technique more relevant. We consider a system operating (1) over short distances of less than 100m between the terminals (so that the processing power is comparable to the transmit power), (2) in slow/block fading channels (so that the channel impulse response remains constant for the duration of an image), and (3) with a low bit-rate feedback channel which correctly updates the channel condition and image variabilities for each image.

In this section, we present \mathcal{S} , \mathcal{C} , and the energy optimization problem for a wireless image transmission system. In section 4.2, models are presented for end-to-end system performance, and energy models are presented for various system components.

2.1 Input State Space

The input state space \mathcal{S} is a collection of all input states or scenarios of interest for which reconfiguration is desired. The size of \mathcal{S} depends upon the input variabilities and the granularity of the reconfigurable hardware. For the problem of wireless image transmission, the inputs which can affect the power consumption or the system performance are the channel response, and the image variability.

Based on our general approach to optimization of image transmission systems with rate and energy constraints in [7], we characterize the image variability in terms of the operational rate-distortion (R-D) curve (see Figure 1(a)). The R-D curve determines the (zero-error) bit-rate necessary to achieve a particular mean-squared error distortion. Characterizing the image variability in terms of the source R-D curve enables us to use a general JSCC formulation of the tradeoff between data and redundancy.

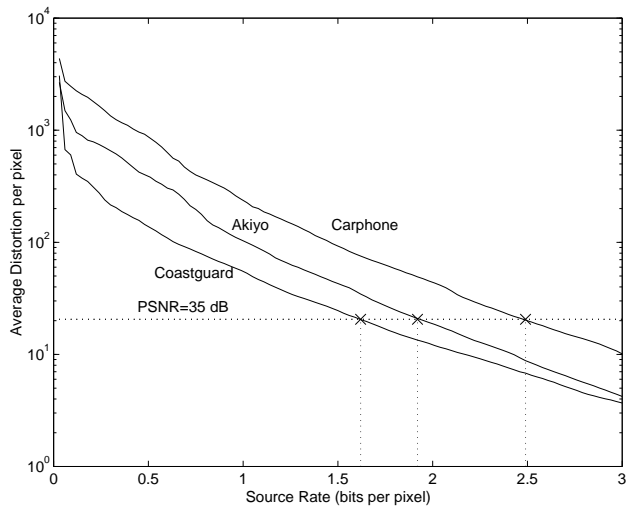
The state vector \mathbf{s} for the wireless image transmission system is:

$$\mathbf{s}=[(r_1, d_1), (r_2, d_2), \dots, (r_K, d_K), h_1, h_2, \dots, h_L], \quad (1)$$

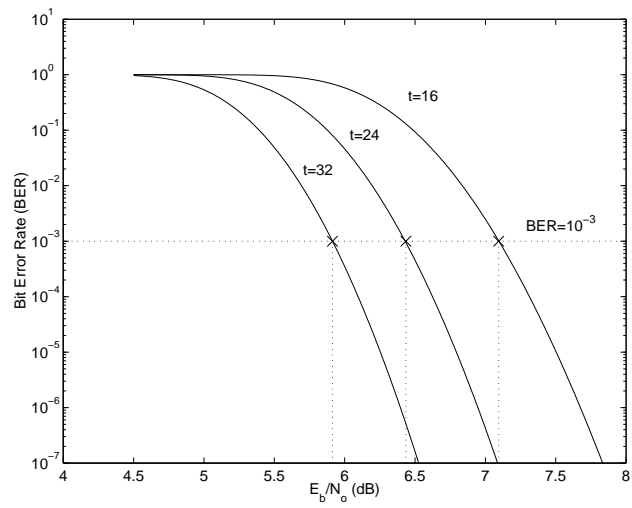
The h_i s are the complex gains in the multipath channel impulse response,

$$h(t) = \sum_{i=1}^L h_i \delta(t - \tau_i), \quad (2)$$

where τ_i is the delay corresponding to the i^{th} path. In addition to multipath, there is typically also multiuser interference which can be exploited by employing a reconfigurable multiuser receiver. In



(a)



(b)

Figure 1: (a) Source variabilities (rate-distortion curves) and (b) channel variabilities (bit-error-rate curves).



Figure 2: Indoor wireless image transmission system.

this paper, for the sake of simplicity, we exploit only the variabilities due to source and multipath channels and consider the worst-case multiuser interference.

2.2 Configuration Space

We must define the set of possible adaptations of the system to the variable input. The configuration space \mathcal{C} is the set of hardware configurations for the terminal. The definition of configuration vector and size of \mathcal{C} depends on the DSP algorithms used in the system and the flexibility of the hardware platform. The maximum benefit of the system optimization approach depends on the size of \mathcal{C} .

For the image transmission problem, we consider the reconfigurable system shown in Figure 3. In this block diagram, the blocks within dotted lines in Figure 3(a) are reconfigurable and the others are fixed/hardwired. The analog and RF blocks (not shown) would include a CDMA modulator, an RF modulator and demodulator, square-root raised cosine filters, an analog-to-digital converter, a digital-to-analog converter and a low-noise amplifier. These blocks are not reconfigurable and are assumed to have fixed energy consumption. The energy consumption due to these blocks is not included in the calculations.

The source codec is implemented on a programmable processor and is assumed to have a fixed energy consumption. All other digital blocks except the source codec are assumed to have an ASIC implementation in $0.18\mu\text{m}$, 2.5V standard-cell CMOS technology.

For the source codec we use the well-known SPIHT coder [13] which has good performance on natural images. For transform-based source coders such as SPIHT, most of the energy consumption is due to the frequency transform or subband decomposition, and energy consumption due to quantization is small. Since the wavelet transform component of the SPIHT coder is fixed, fixed energy consumption is a good assumption.

For the channel codec, we employ Reed-Solomon block codes to provide error correction for bursty error channels. In section 4.1, we describe a reconfigurable architecture for the codec in which the energy consumption is proportional to the redundancy added by the codec.

The power limitations of the terminal depend on whether it is a mobile or a base station. A mobile utilizes battery power which has limited life, whereas a base has access to a stationary power source with unlimited life. We assume that both mobiles and bases have a fixed maximum transmit power. The configuration vectors for the mobile (\mathbf{m}) and the base-station (\mathbf{b}), respectively, are

defined as follows:

$$\mathbf{m} = [R_s, t_{enc}, P_t, \mathbf{c}_{rake}, t_{dec}] \quad (3)$$

$$\mathbf{b} = [R_s, t_{enc}, t_{dec}], \quad (4)$$

where R_s is the source rate (in bits per pixel), t_{enc} is the maximum number of correctable symbol symbols per block at the channel encoder, P_t is the transmit power (or output power delivered by the power amplifier), and \mathbf{c}_{rake} is the configuration vector for the RAKE receiver ($c_{rake,i} = 0$ implies that i^{th} finger is powered down). The transmit parameters of the mobile are R_s , t_{enc} , and P_t . The receive parameters of the mobile are the number of protection symbols per block at the channel decoder t_{dec} , and \mathbf{c}_{rake} . The parameter \mathbf{c}_{rake} depends on the transmit power of the other device and the channel condition, and t_{dec} is same as t_{enc} of the other device (either the base-station or the other mobile). Further, \mathcal{M} and \mathcal{B} are the configuration-spaces (defined as set of all possible configuration vectors) for the mobile and base-station, respectively.

Figure 3(b) shows the block diagram of the controller. The controller adapts the system to the changes in the input by reconfiguring or changing the parameters of the various blocks. The first block in the controller quantizes the input variabilities as determined by the source coder and channel decoder. The energy-optimum configuration vectors are either obtained by an optimization algorithm running in real-time or from a precalculated look-up table.

2.3 Energy Optimization Problem

We develop the energy optimization problem by expressing the total energy consumption and end-to-end performance of the system in terms of the system configuration and the given input. We first describe the general optimization problem for terminal to terminal communication, then follow up with simplifications for different scenarios. The most general problem is two-way mobile-to-mobile communication, since the configuration vector for the base is a special case of the mobile configuration vector where the transmit power and number of RAKE fingers are free variables.

2.3.1 General optimization scenario : mobile-to-mobile scenario

Consider two-way mobile-to-mobile communication. The state vectors for the system, \mathbf{s}_{m1} and \mathbf{s}_{m2} , describe: (1) the rate-distortion points of the image transmitted by *mobile*₁, and the channel response from *mobile*₁ to *mobile*₂, and (2) the rate-distortion points of the image transmitted

by *mobile*₂, and the channel response from *mobile*₂ to *mobile*₁, respectively. We determine the configuration vectors, $\mathbf{m1}_{opt}(\mathbf{s}_{m1})$ and $\mathbf{m2}_{opt}(\mathbf{s}_{m2})$, which minimize the energy consumption per pixel at each mobile while satisfying constraints on (1) distortion \mathcal{D}_{m1} per pixel for the image transmitted by *mobile*₁ (distortion is defined as mean-squared error between the original image at the transmitter input and the reconstructed image at the receiver output) and distortion \mathcal{D}_{m2} per pixel for the image transmitted by *mobile*₂, and (2) total rate $R_{m1,tot}$ and $R_{m2,tot}$ (total rate is defined as the sum of source and channel bits per pixel) at *mobile*₁ and at *mobile*₂, respectively. Therefore, the energy optimization problem can be written as

$$\begin{aligned}
(\mathbf{m1}_{opt}(\mathbf{s}_{m1}), \mathbf{m2}_{opt}(\mathbf{s}_{m2})) &= \arg \min_{\mathbf{m1} \in \mathcal{M}, \mathbf{m2} \in \mathcal{M}} \mathcal{E}(\mathbf{m1}, \mathbf{m2}) \\
s.t. \quad \mathcal{D}_{m1}(\mathbf{m1}, \mathbf{s}_{m1}) &\leq \mathcal{D}_{o1}, \\
\mathcal{D}_{m2}(\mathbf{m2}, \mathbf{s}_{m2}) &\leq \mathcal{D}_{o2}, \\
R_{m1,tot}(\mathbf{m1}) &\leq R_{o1}, \\
R_{m2,tot}(\mathbf{m2}) &\leq R_{o2},
\end{aligned} \tag{5}$$

where $\mathcal{E}(\mathbf{m1}, \mathbf{m2})$ is the sum of the energy consumption at each mobile $\mathcal{E}(\mathbf{m1}, \mathbf{m2}) = \mathcal{E}_{m1}(\mathbf{m1}, \mathbf{m2}) + \mathcal{E}_{m2}(\mathbf{m1}, \mathbf{m2})$.

The energy consumption at *mobile*₁ is given by

$$\mathcal{E}_{m1}(\mathbf{m1}, \mathbf{m2}) = \mathcal{E}_{rsenc}(t_{enc}^{m1}) + \mathcal{E}_{rsdec}(t_{enc}^{m2}) + \mathcal{E}_{rake}(\mathbf{c}_{rake}) + \mathcal{E}_{pa}(P_t) + \mathcal{E}_{fixed}, \tag{6}$$

where \mathcal{E}_{rsenc} , \mathcal{E}_{rsdec} , \mathcal{E}_{rake} , \mathcal{E}_{pa} , and \mathcal{E}_{fixed} are the energy consumption of the RS encoder, RS decoder, RAKE receiver, power amplifier, and fixed components respectively. The RS encoder power consumed in the mobile is for encoding the data to be transmitted. The RS decoder power consumed at *mobile*₁ is for decoding the received data from *mobile*₂. At present, we do not include \mathcal{E}_{fixed} due to the source encoder and the other hardwired blocks in the optimization problem. Any flexibility in these fixed system components would increase the benefits of an optimization approach. The optimization problem in (5) represents the core of DAT where energy is minimized subject to a system-level performance constraint. The constraints themselves are satisfied via joint source-channel coding algorithms.

Assuming that the two users are exchanging independent information, the energy optimization above can be partitioned into two one-way communication problems, one for each direction. For

the image transmitted from $mobile_1$ to $mobile_2$,

$$\begin{aligned}
[R_s, t_{enc}^{m1}, P_t, \mathbf{c}_{rake}]_{opt} &= \arg \min \mathcal{E}_{rsenc}(t_{enc}^{m1}) + \mathcal{E}_{rsdec}(t_{enc}^{m1}) + \mathcal{E}_{rake}(\mathbf{c}_{rake}) + \mathcal{E}_{pa}(P_t) \\
s.t. \quad \mathcal{D}_{m1}(\mathbf{m1}, \mathbf{s}_{m1}) &\leq \mathcal{D}_{o1}, \\
R_{m1,tot}(\mathbf{m1}) &\leq R_{o1}.
\end{aligned} \tag{7}$$

$Mobile_1$ receives channel information from $mobile_2$ and uses it to compute R_s, t_{enc}^{m1}, P_t for its own configuration as well as \mathbf{c}_{rake} for $mobile_2$. $Mobile_2$ combines the \mathbf{c}_{rake} information transmitted by $mobile_1$ with R_s, t_{enc}^{m2}, P_t to obtain its configuration vector. An optimization algorithm for determining the configuration vectors $\mathbf{m1}_{opt}$ and $\mathbf{m2}_{opt}$ is described in the next section.

A performance criterion which may be more desirable to the end user is the probability of delivering a particular quality of service. The user may desire that the distortion is above some level \mathcal{D}_o with probability \mathcal{P}_o which is close to zero. The optimization problem then becomes

$$\begin{aligned}
(\mathbf{m1}_{opt}(\mathbf{s}_{m1}), \mathbf{m2}_{opt}(\mathbf{s}_{m2})) &= \arg \min_{\mathbf{m1} \in \mathcal{M}, \mathbf{m2} \in \mathcal{M}} \mathcal{E}(\mathbf{m1}, \mathbf{m2}) \\
s.t. \quad P(\mathcal{D}_{m1}(\mathbf{m1}, \mathbf{s}_{m1}) > \mathcal{D}_{o1}) &\leq \mathcal{P}_{o1}, \\
P(\mathcal{D}_{m2}(\mathbf{m2}, \mathbf{s}_{m2}) > \mathcal{D}_{o2}) &\leq \mathcal{P}_{o2}, \\
R_{m1,tot}(\mathbf{m1}) &\leq R_{o1}, \\
R_{m2,tot}(\mathbf{m2}) &\leq R_{o2},
\end{aligned} \tag{8}$$

This problem separates into an optimization problem for the image transmitted by $mobile_1$ and an optimization problem for the image transmitted by $mobile_2$, where $P(\mathcal{D} > \mathcal{D}_o)$ is the probability that the rate corresponding to the desired maximum distortion \mathcal{D}_o is successfully decoded. Joint source-channel coding does not play a significant role in this situation because the source coder must operate at a specified rate R_s (as determined by the rate-distortion points) and the channel codec is energy-optimized. In this scenario, it is possible that for large values of \mathcal{P}_o and \mathcal{D}_o , the bandwidth is under-utilized.

2.3.2 Special Case: Mobile-to-Base-Station Scenario

Consider two-way communication between a mobile and a base station. The optimization problem for the system is just a special case of (5) in which one of the mobiles, say $mobile_2$, is a base-station. As in the mobile-to-mobile scenario, the system optimization divides into two problems,

one for the base station, and one for the mobile. Because the power consumption at the base station is not considered an issue here, these problems are special cases of the problem in (7) with $\mathcal{E}_{rsenc}(t_{enc}^{m2})$, $\mathcal{E}_{rsdec}(t_{enc}^{m1})$, and $\mathcal{E}_{rake}(\mathbf{c}_{rake})$ at the base station all set to zero. Otherwise, the optimization problem and the algorithm with solution remain the same as in the general case. So, for the image transmitted from the mobile over the uplink channel,

$$\begin{aligned}
[R_s, t_{enc}^m, P_t]_{opt} &= \arg \min \mathcal{E}_{rsenc}(t_{enc}^m) + \mathcal{E}_{pa}(P_t) \\
s.t. \quad \mathcal{D}_m(\mathbf{m}, \mathbf{s}_m) &\leq \mathcal{D}_o, \\
R_{m,tot}(\mathbf{m}) &\leq R_o.
\end{aligned} \tag{9}$$

2.3.3 Optimization Example

To illustrate the necessity of the optimization and to clarify our methodology, we provide the simple example of one-way mobile-to-mobile communication with a configuration space of three choices. Figure 4 shows the total energy consumed ($\mathcal{E}_{rsenc} + \mathcal{E}_{rsdec} + \mathcal{E}_{rake} + \mathcal{E}_{pa}$) at distances of 10m and 50m for images “*carphone*” and “*coastguard*” by the three different configurations m_1 , m_2 , and m_3 with the parameters listed in Table 1. Note that R_s is not listed, since it is related to t_{enc} by the rate constraint $R_{tot} \leq R_o$.

Configuration	t_{enc}	P_t (mW)	$\sum_i c_{rake,i}$	$\mathcal{E}_{tot}(mJ)$
m_1	4	0.01	1	0.0592
m_2	44	0.4	2	0.3600
m_3	34	0.466	2	0.3680

Table 1: Configuration space parameters.

Configuration m_1 supports a PSNR= 35dB for both images at 10m, but not at 50m. Configuration m_2 supports “*coastguard*” at 50m and 10m, but does not support “*carphone*” at either distance because the rate R_{tot} is too small. Configuration m_3 supports both images at both distances, but is not energy-efficient for short distances. Because of image variability and channel variability, reconfiguration is required for energy efficiency. Optimal configuration parameters can be determined either by brute-force search or with an optimization algorithm. When the sizes of the configuration space and the input state space are small, a brute-force search is feasible; otherwise, an optimization algorithm is required. In this paper, the configuration space has a size of

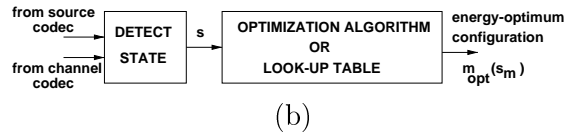
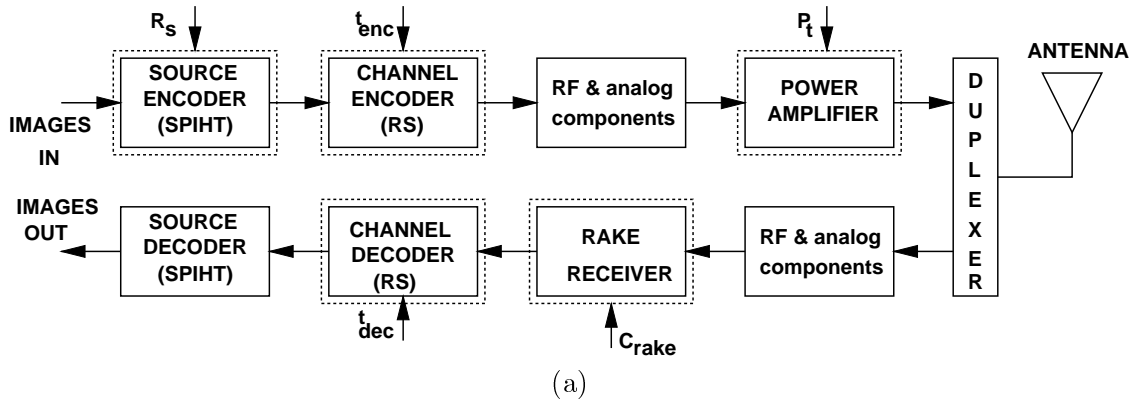


Figure 3: A reconfigurable multimedia system: (a) the transceiver and (b) the controller.

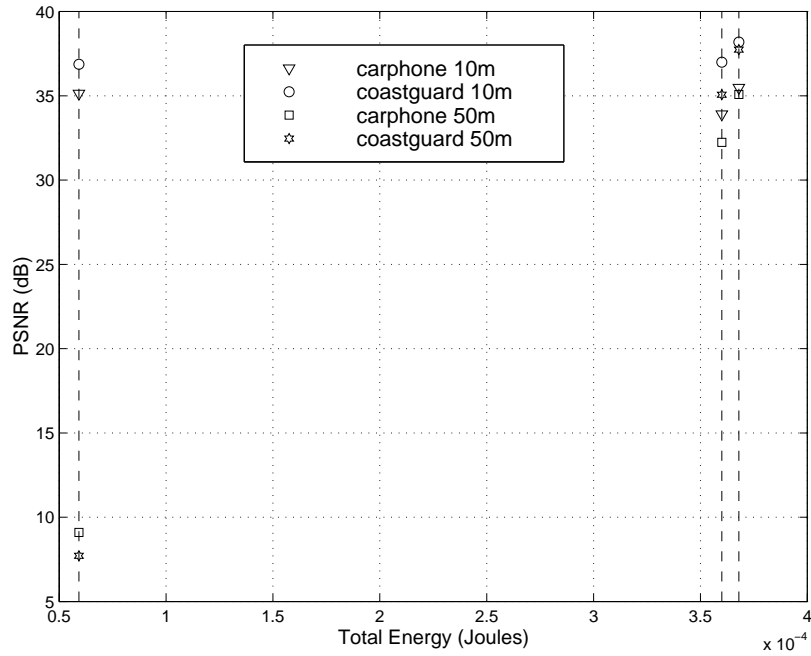


Figure 4: Performance of three configurations m_1 , m_2 and m_3 defined in Table 1.

$|\mathcal{M}| = 127 \times 256 \times 6 = 195\,072$ corresponding to the variation in protection symbols \times variation in P_t \times the variation in \mathbf{c}_{rake} and the state space has a size of $9\,504 \times 6 = 57\,024$ corresponding to the number of rate-distortion points \times the length of the channel response.

3 Optimization Algorithm

All the energy optimization problems described are solved by a feasible directions algorithm [15]. At each step of the algorithm, the gradient ∇E of the objective function $E(t_{enc}^m, P_t)$ is taken with respect to t_{enc}^m and P_t and a feasible direction $d = [d(1), d(2)]$ is chosen so that the objective function decreases (i.e $\nabla E d' \leq 0$). The update at each step is

$$[t_{enc}^m, P_t]_{k+1} = [t_{enc}^m, P_t]_k + [d(1), d(2)] \quad (10)$$

$$d(2) = \left(\alpha - \frac{dE}{dt} d(1) \right) / \frac{dE}{dP_t} \quad (11)$$

The derivatives in (11) are computed numerically as $\frac{dE}{dt} = E(t + 1, P_t) - E(t, P_t)$ and $\frac{dE}{dP_t} = \frac{E(t, P_t + P_{t,min}) - E(t, P_t)}{P_{t,min}}$, where $P_{t,min}$ is the minimum transmit power. The parameters $\alpha > 0$, and $d(1) > 0$ determine the stepsize and the angle between the direction and the gradient, respectively. For the image transmission system studied here, we chose $\alpha = P_{t,min}$, and $d(1) = 1$ to be a unit step.

Taking a step in the feasible direction does not guarantee that the distortion constraint is met. Assuming that we start at an initial state $[t_{enc}^m, P_t]_0$ which satisfies the constraint, at each update, the distortion is measured and compared to the constraint. If the distortion constraint is not met, then the update is not taken and the stepsize α is decreased towards zero until the distortion constraint is met. For the image transmission system studied here, we chose the modification $\alpha = 0.9\alpha$, and reset the parameter to $\alpha = P_{t,min}$ for each new gradient computation. Many variations of this simple feasible directions algorithm are possible.

To determine the optimal \mathbf{c}_{rake} , we apply the optimization algorithm for each of the possible values and choose the best one. To apply the optimization algorithm to the $P(\text{fail})$ case, the distortion constraint is replaced with the probability constraint

$$P(R < R_{\mathcal{D}_o}) < \mathcal{P}_o, \quad (12)$$

where R is the number of consecutive bits decoded correctly, and $R_{\mathcal{D}_o}$ is the rate corresponding to distortion \mathcal{D}_o , as determined by the rate-distortion points.

The energy and performance models employed in the estimation of $\mathcal{E}(\mathbf{m}, \mathbf{b})$, $\mathcal{E}(\mathbf{m1}, \mathbf{m2})$, $\mathcal{D}(\mathbf{m}, \mathbf{s}_m)$, and $\mathcal{D}(\mathbf{b}, \mathbf{s}_b)$ are described next.

4 Energy and Performance Models

In this section, we present relationships of the energy consumption and distortion to the configuration signals. The high-level estimates of the energy consumption are obtained via energy models for the power-hungry blocks in the RS codec, RAKE receiver, and power amplifier. These models are obtained via real-delay simulations [16] of the hardware blocks employing $0.18\mu m$, $2.5V$ CMOS standard cells obtained from [17]. Similarly, performance models of the source coder and the channel coder are employed to estimate the average distortion per pixel for the various states and configurations.

4.1 Energy Models

Energy models are employed to relate the configuration vector to a high-level estimate of the energy consumption of the algorithm. It is well known that the energy consumption of the digital circuits is dependent upon the input signal statistics. However, in the case of Galois field multipliers and adders, it is found that the energy consumption varies by less than 5%, when the correlation of the input bit-stream is varied from 0.0 to 0.9. This is because when the correlated bit-stream is converted to Galois field symbols, the correlations among successive bits are lost, thus making Galois field symbols uncorrelated. Therefore, in the following, we present energy models which are independent of the input signal statistics, but are functions of input precisions. The energy models for the RS codec, the RAKE receiver, and the power amplifier are presented next.

1. RS Encoder/Decoder

The complete block diagram of the Galois field components and the RS encoder and decoder are derived in the Appendix and can also be found in [18]. We summarize the results here to maintain the flow of the discussion. The energy models for adder, multiplier and inverse blocks over Galois field $GF(2^m)$ are derived by simulating these blocks via a real-delay gate-level simulator MED [16] and are given by

$$\mathcal{E}_{gfadd} = 3.3 \times 10^{-5} m \quad (mW/MHz) \quad (13)$$

$$\mathcal{E}_{gfmult} = 3.7 \times 10^{-5} m^3 \quad (mW/MHz) \quad (14)$$

$$\mathcal{E}_{gfinv} = 3.7 \times 10^{-5} (2m - 3)m^3 \quad (mW/MHz), \quad (15)$$

where m is the number of bits per symbol. These models are employed to obtain an estimate of the energy consumption of the RS encoder and decoder in different configurations. The energy consumption of a bit-parallel RS encoder architecture is given by

$$\mathcal{E}_{rsenc}(t) = 2t(2^m - 1 - 2t) (\mathcal{E}_{gfmult} + \mathcal{E}_{gfadd}) / \text{codeword}. \quad (16)$$

Energy consumption of the RS decoder is due to the syndrome computation (SC) block, Berlekamp-Massey (BM) block and Chien-Forney (CF) block and is given by

$$\mathcal{E}_{rsdec}(t) = 4t(2^m - 1 + 5t/2)\mathcal{E}_{gfmult} + 4t(2^m - 1 + 3t/2)\mathcal{E}_{gfadd} + 3t\mathcal{E}_{gfinv} / \text{codeword}. \quad (17)$$

The energy consumption of the RS codec is obtained as a sum of \mathcal{E}_{rsenc} and \mathcal{E}_{rsdec} in (16) and (17) as follows:

$$\mathcal{E}_{rscodec}(t) = 6t(2^m - 1 + t)\mathcal{E}_{gfmult} + 6t(2^m - 1 + t/3)\mathcal{E}_{gfadd} + 3t\mathcal{E}_{gfinv} / \text{codeword}. \quad (18)$$

2. RAKE Receiver

Energy consumption of the RAKE receiver in Figure 5(a) is dependent upon the powered-up fingers (i.e., taps for which $c_{rake,i} = 1$). Figure 5(b) shows the architecture of a finger in a RAKE receiver. The received signal $r[n]$ is correlated with the delayed spreading sequences $s_i = s[n - \tau_i]$ and then multiplied by a complex gain h_i^* . The outputs from all the fingers are added together and passed to the slicer to obtain the bits. If L is the number of fingers, then the energy consumption of the RAKE receiver is given by

$$\mathcal{E}_{rake}(\mathbf{c}_{rake}) = \sum_{i=0}^{L-1} c_{rake,i} \mathcal{E}_{rake,i} / \text{bit}, \quad (19)$$

where $\mathcal{E}_{rake,i}$ is the energy consumed by the i^{th} finger of the RAKE receiver. The adder and multiplier energy models [5] are obtained via real-delay gate-level simulations of the blocks designed for $0.18\mu m$, $2.5V$ CMOS technology from [17].

3. Power Amplifier

Energy consumption of the power amplifier is characterized by its power-aided-efficiency (PAE) η (defined as the ratio of the output power P_t to the power drawn from the supply). Power amplifiers are typically designed to maximize η at the maximum output power $P_{t,max}$, with η being

a decreasing function of P_t . The functional relationship between η and P_t (also called a power-aided-efficiency curve) is usually provided in vendor data-books. For the digitally-programmable power amplifier in [19], the efficiency $\eta(P_t)$ of this power amplifier can be approximated as follows:

$$\eta(P_t) = \eta_{max} \sqrt{\frac{P_t}{P_{t,max}}}, \quad (20)$$

where η_{max} is the maximum efficiency, and $P_{t,max}$ is the maximum transmit power. If f_{bit} is the bit-rate, then the power amplifier energy consumption per bit \mathcal{E}_{pa} is given by

$$\mathcal{E}_{pa}(P_t) = \frac{P_t}{f_{bit}\eta(P_t)} / bit. \quad (21)$$

4.2 Rate Models

Performance models are employed to relate the configuration vector to the performance metrics such as distortion, bit error rate (*BER*) or signal-to-noise ratio (*SNR*). In the following, we present performance models for the source coder, channel coder, RAKE receiver and power amplifier.

1. Source Coder

The performance metric for the image transmission system is the end-to-end average distortion per pixel. The SPIHT source coder produces a progressive bitstream which improves the quality of the decoded image as more bits are received correctly. When a bit error occurs in the transmission, all future bits are lost due to an embedded property of the bitstream. So, the end-to-end average distortion per pixel can be computed [7] as follows:

$$\mathcal{D}(\mathbf{s}, \mathbf{c}) = \sum_{i=0}^{M-1} D(i)p(i) + D(M) \prod_{i=0}^{M-1} (1 - p(i)), \quad (22)$$

where M is the number of codewords transmitted per image, $D(i)$ is the distortion value if only the first i codewords are correctly received, $p(i)$ is the probability of receiving the first i codewords correctly and the $(i+1)^{th}$ codeword in error, and $D(M)$ is the residual distortion because of a finite source rate R_s . The $D(i)$ values are obtained from the image-specific operational rate-distortion curve of the SPIHT coder. The $p(i)$ values are obtained from the error probability of the channel code. For block-error codes, the probability of receiving i consecutive blocks correctly is given by:

$$p(i) = (1 - p_{e,c})^i p_{e,c}, \quad (23)$$

where $p_{e,c}$ is the probability of error for the channel code.

2. Source Estimation: Operational Rate-Distortion

The variability in the input data is captured by operational rate-distortion points. There are several ways of estimating these rate-distortion points. The straight-forward approach is to apply the source encoder and decoder at various rates, calculate the distortion between the original and decoded images, and interpolate between these (r, d) points. In [20], Lin et al. use a cubic spline interpolation to get smooth rate-distortion curves for gradient-based optimization algorithms. Since multiple (r, d) points must be measured by encoding and decoding at these rates, the processing power required for the computation is significant.

We consider some simplifications and special cases. For transform-based source coders such as SPIHT and JPEG, the error in the encoded image is primarily due to quantization, especially at high rates. The transform-domain quantization error energy at various rates provides an estimate of the operational rate-distortion points. In the SPIHT coder, wavelet transform coefficients are encoded hierarchically according to bit-planes, starting from the most significant bit-plane. The compressed bitstream has the embedded property of containing all the lower rates. Due to the embedded nature of this compressed bitstream, shortening the compressed bitstream is the same as compressing to the lower rate. In terms of estimating the (r, d) points, this implies that the encoder need only be run at the maximum rate.

We can compute the error energy at the encoder progressively from lower rates to higher rates as follows. Let $\{c_1^0, c_2^0, \dots, c_D^0\}$ be the set of original wavelet coefficients, where D is the number of pixels in the image. Let n be the number of bits to encode the largest coefficient. At zero source rate, the distortion energy $E_0 = \sum_{i=1}^D (c_i^0)^2$ is the total energy in the wavelet coefficients. When the most significant bit-plane is encoded, the new distortion energy $E_1 = \sum_{i=1}^D (c_i^1)^2$, where the coefficients are

$$c_i^1 = c_i^0 - I(c_i^0)2^{n-1} \quad (24)$$

$$I(c_i^0) = \begin{cases} 1 & \text{if } c_i^0 \geq 2^{n-1} \\ 0 & \text{otherwise} \end{cases} \quad (25)$$

The indicator function $I(c)$ just determines whether the particular coefficient c has a 1 in the most-significant bit-plane. By expanding and collecting terms, we can write

$$E_1 = E_0 - 2^{n-1} \left(2 \sum_{i=1}^D I(c_i^0) c_i^0 - M 2^{n-1} \right), \quad (26)$$

where $M = \sum_{i=1}^D I(c_i^0)$ is the number of coefficients with a 1 in the most-significant bit-plane. For the coefficients not being updated, $I(c) = 0$, so the summation is over relatively few values. The summation can easily be computed by shifting the coefficients being updated, masking off the error, and accumulating (M does not have to be computed explicitly). For the next most significant bit-plane, we update E_1 based on the number of coefficients with 1 at this bit-plane and so on. The introduction of this calculation does not require any additional memory, since only the original coefficient values need to be accessible. To convert error energy to distortion, we simply divide by the number of total image pixels. The rate at which a particular distortion occurs is known as a consequence of the encoding (length of the output buffer). We also point out the update above can occur at finer steps than at each bit-plane. So, the complete rate-distortion curve can be found using this technique in real-time to progressively update the error energy as more significant bits are encoded.

3. Channel Coder

The performance metric for the channel coder is the probability of error $p_{e,c}$. For a Reed-Solomon code with codeword length of $2^m - 1$ symbols and error correction capability of t symbols, we have [21]

$$p_{e,c} = \sum_{j=t+1}^{2^m-1} \binom{2^m-1}{j} p_{e,s}^j (1 - p_{e,s})^{2^m-1-j}, \quad (27)$$

where $p_{e,s}$ is the symbol error probability and is computed as:

$$p_{e,s} = 1 - (1 - p_{e,b})^m, \quad (28)$$

where $p_{e,b}$ is the uncoded bit error probability computed as (for AWGN channels and binary phase shift signaling scheme) [22]

$$p_{e,b} = Q[\sqrt{SNR_o}], \quad (29)$$

where SNR_o is the signal-to-noise ratio at the output of the RAKE receiver, and $Q[x]$ is the probability that a standard Gaussian random variable has value greater than x .

4. Power Amplifier and RAKE Receiver

The performance for the power amplifier and RAKE receiver is defined by SNR_o and is computed as:

$$SNR_o = \frac{P_t PL(d)}{P_n} \sum_{i=0}^{L-1} c_{rake,i} |h_i|^2, \quad (30)$$

where P_t and P_n are the transmit power and noise power, respectively, $PL(d)$ is the propagation loss for distance d between the transmitter and receiver, L is the number of fingers in the RAKE receiver, $c_{rake,i}$ is the configuration signal for i^{th} RAKE finger, and h_i is the channel coefficient for the i^{th} path.

5 Application to Indoor Office Channels

In this section, we simulate the proposed reconfigurable multimedia system in an indoor office environment. Our goals are to determine the improvement obtained in a realistic setting using our total system optimization. We compare with both conventional worst-case fixed design and a system employing power control. We find that significant power reduction is possible in the short range. These results are understood better by studying more detailed behavior such as comparing the power amplifier power consumption with the power consumption of the digital blocks, power consumption of the individual blocks, and the variability of the optimal parameters over the images and over distance. Section 5.1 presents the simulation setup and simulation results follow in section 5.2.

5.1 Simulation Setup

The proposed receiver is simulated for an indoor office environment. The propagation models for indoor office channels are obtained from the IMT-2000 evaluation methodology [14]. In these models, the propagation effects are divided into two distinct types: (1) mean path loss and (2) variation in the signal due to multipath effects. The mean path loss PL for the indoor office environment is modeled as follows:

$$PL(d) = 37 + 30 \log_{10} d + 18.3q^{\left(\frac{q+2}{q+1}-0.46\right)} \text{ (in dB)}, \quad (31)$$

where d is the transmitter and receiver separation (in meters) and q is number of floors in the path. This represents a worst-case model from an interference point of view. We assume that distance d can vary from $2m$ to $100m$.

The multipath effect is modeled via a channel impulse response which is characterized by a delay-line model given in (2). The mean values of the relative delays (τ_i) and relative power ($|h_i|^2$) are specified in Table 2 [14]. Channel models A and B are the low delay spread and median

delay spread cases, respectively. Each of these two channels can occur in an actual scenario with probability of 45 – 50%.

Path	Channel A		Channel B	
	Relative delay (ns)	Average power (dB)	Relative delay (ns)	Average power (dB)
1	0	0	0	0
2	50	-3.0	100	-3.6
3	110	-10.0	200	-7.2
4	170	-18.0	300	-10.8
5	290	-26.0	500	-18.8
6	310	-32.0	700	-25.2

Table 2: Indoor office multipath channels [14].

We assume that we are transmitting a database of images with 176×144 pixels per frame in *quarter common intermediate format (QCIF)* obtained from [23].

It was found that a PSNR of $35dB$ provided a desirable level of visual quality and a total rate R_o of $3 \text{ bits per pixel (bpp)}$ is sufficient to obtain this PSNR. Some other system parameters are given in Table 3.

Rates	Frame Rate	10 <i>frames/sec</i> @ 3 <i>bpp</i> (176×144 pixels QCIF images)
	Bit rate	760.32 <i>kbits/sec</i> (binary phase shift keying)
	Chip rate	12.16 <i>Mchips/sec</i> (length 16 spreading sequences)
Power Amplifier	Maximum efficiency $\eta_{max} = 50\%$	Low Power: $P_{t,max} = 50 \mu W$ High Power: $P_{t,max} = 5 mW$
RAKE receiver and Channel Codec	0.18 μ , 2.5V CMOS Technology	
Low-noise amplifier	Noise figure=5 <i>dB</i> , B.W.=12.16 <i>MHz</i>	
Constraints	\mathcal{D}_o	30 <i>dB</i> or 35 <i>dB</i> (in terms of PSNR)
	R_o	3 <i>bits per pixel (bpp)</i>

Table 3: System parameters.

5.2 Simulation Results

The real novelty/impact of the work is shown by the difference in power consumption between optimized and fixed systems. The energy savings are obtained by reconfiguring the system to take advantage of image and channel variabilities. The contribution of the input variability to the reconfiguration is shown in the variation of the parameters in the configuration vector.

The proposed mobile-to-mobile image transmission system is tested for distances from $2m$ to $100m$, multipath channels A and B described in the previous subsection, QCIF images “*akiyo*”, “*carphone*”, “*claire*”, “*coastguard*”, “*container*”, “*hall_objects*”, “*mother_and_daughter*” and “*silent*”, total rate R_o of 3 bps , and PSNR of 35dB .

To show the overall impact of the optimization approach, we compare the optimized system to two fixed systems for the end-to-end distortion criterion and the $P(\text{fail})$ criterion. Then, the contribution of each component of the system is analyzed in detail to show the origin of the power-consumption savings.

1. Comparison with Fixed Systems

Figure 6 shows a comparison between the long-range optimized system and the long-range transmit-power-controlled system (averaged over both channels, all the images, and both PSNR constraints) where both systems employ the high-power amplifier designed for long distances. A significant point is that the fixed system is not a worst-case comparison. The fixed system utilizes the feedback channel to account for the variation of transmit power over distance but does not account for the variation in the digital block parameters (as in the optimized system). The average total power savings of 15.6% between the two systems arises due to reconfiguration of the source rate, RS coder, and RAKE fingers.

The power amplifier at the transmitter is a significant component of the power consumption in the image transmission system. The efficiency of the power amplifier ranges from 2.2% at the lowest transmit power to its highest efficiency of $\eta_{max} = 50\%$ at the maximum transmit power, $P_{t,max}$. When operating the system over distances from $2m$ to $100m$, the significant variation in transmit power from $10\mu\text{W}$ to 5mW lowers the efficiency of the entire system. A plausible alternative is to use a low-power amplifier for short distances and a high-power amplifier for longer distances.

Figure 7 shows a comparison between the short-range optimized system and the short-range transmit-power-controlled system. The average total power savings due to optimization is 49.4% . Comparing Figure 7 with Figure 6, we see that the low-power transmission system consumes less than one-third of the total energy consumed in the original system designed for longer distances. For this particular system, the choice of the power amplifier plays the most significant role in the efficiency of the transmission system.

Now, we compare the optimized system to a worst-case system which does not employ power

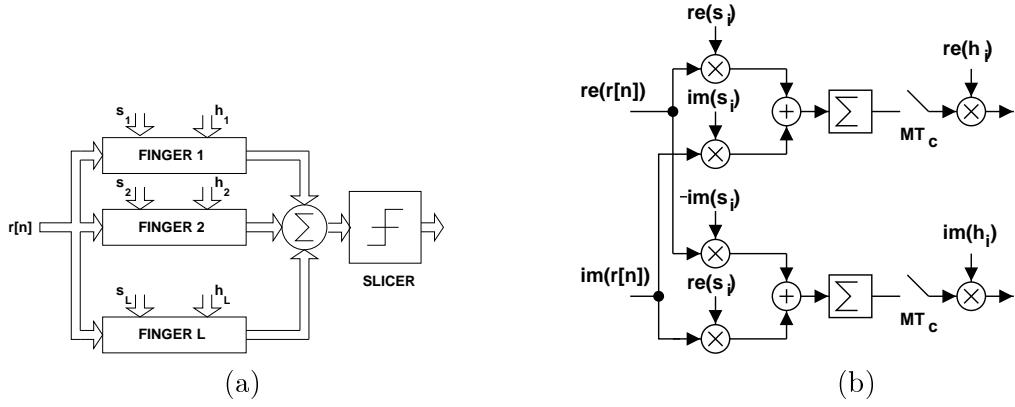


Figure 5: The RAKE receiver: (a) block diagram and (b) architecture of a finger.

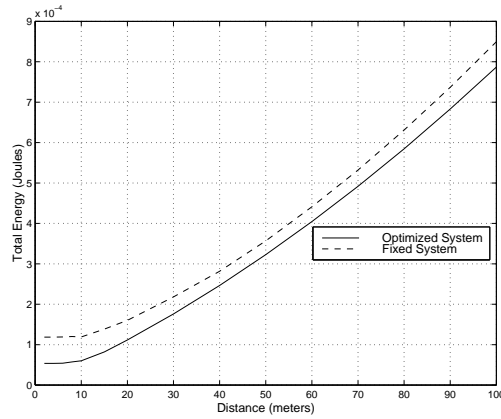


Figure 6: Comparison between transmit-power-controlled system and optimized system over long range.

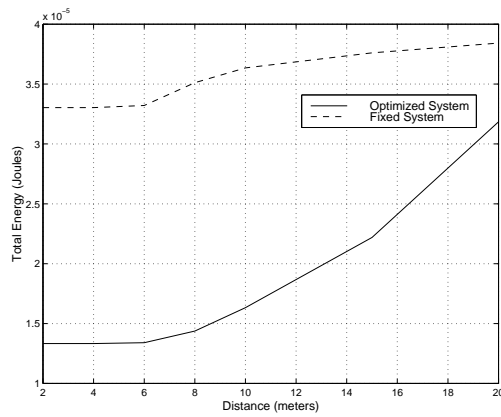


Figure 7: Comparison between transmit-power-controlled system and optimized system over short range.

control. Figure 8 shows a comparison of the PSNR (averaged over both channels and all the images) in the optimized system designed for $30dB$ and $35dB$ and a fixed system designed for the worst-case image, maximum distance, and worst-case channel. The fixed system has constant performance of at least $0.7dB$ above the optimized system, which achieves the PSNR constraint nearly with equality. Although the fixed system performs slightly better than the optimized system in terms of PSNR, it consumes three times more energy.

2. Fraction of total energy consumed in each component

The fraction of energy consumption in each component of the transmission system is shown in Figure 9. At short distances, the RAKE receiver and transmit power are the most significant since the $BERs$ at this distance are relatively low so as to not require additional channel coding. At a distance of $20m$, the fraction of digital energy reaches a peak of 29%, where the RS coder is able to lower $BERs$ by introducing channel coding. At distances over $20m$, the fraction of digital energy decreases since more transmit energy is required to compensate for path loss. More complex channel coding techniques such as convolutional coding for the inner system may be used to increase the range of distances over which digital power consumption is significant and hence benefit from the techniques presented here.

3. Variation of t and P_t

Figures 10 and 11 show the variation of the optimal parameters for the reconfigured system over distance and over the various images. The significant variation of the t and P_t parameters at large distances shows the necessity of an optimization algorithm for those parameters. The optimal number of RAKE fingers is found to be either 1 for short distances or 2 for long distances. The number of RAKE fingers makes a significant impact on the total power consumption since the RAKE consumes significant power. In addition, the variation of the number of RAKE fingers also affects the $Energy/bit$ and consequently the other parameters.

4. $P(fail)$ -Optimized Systems

The energy consumption due to the various blocks is shown in Figure 12 for the constraints $P(PSNR < 30) < 0.01$, $P(PSNR < 30) < 0.1$, $P(PSNR < 35) < 0.01$, and $P(PSNR < 35) < 0.01$ averaged over all the images for $R_o = 3 bpp$, and Channel A. The energy consumption of the RAKE receiver is the same for all the four constraints and constant over the short distances (less than $15m$) and long distances (over $15m$). For the $PSNR = 35dB$ constraint, the energy consumption in

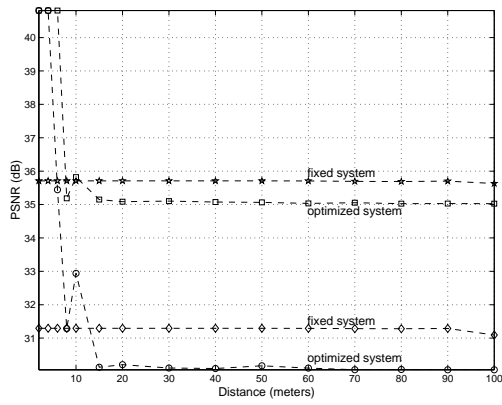


Figure 8: Comparison between fixed system and optimized system performance.

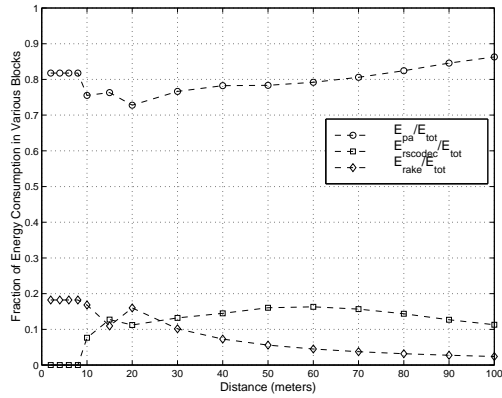


Figure 9: Fraction of energy consumed in each component.

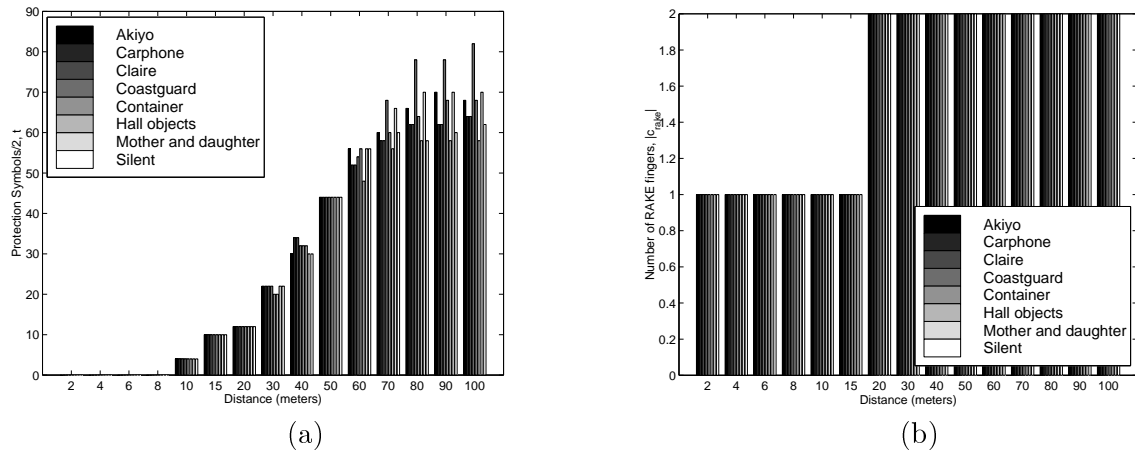


Figure 10: Optimized system parameters: (a) protection symbols and (b) RAKE fingers.

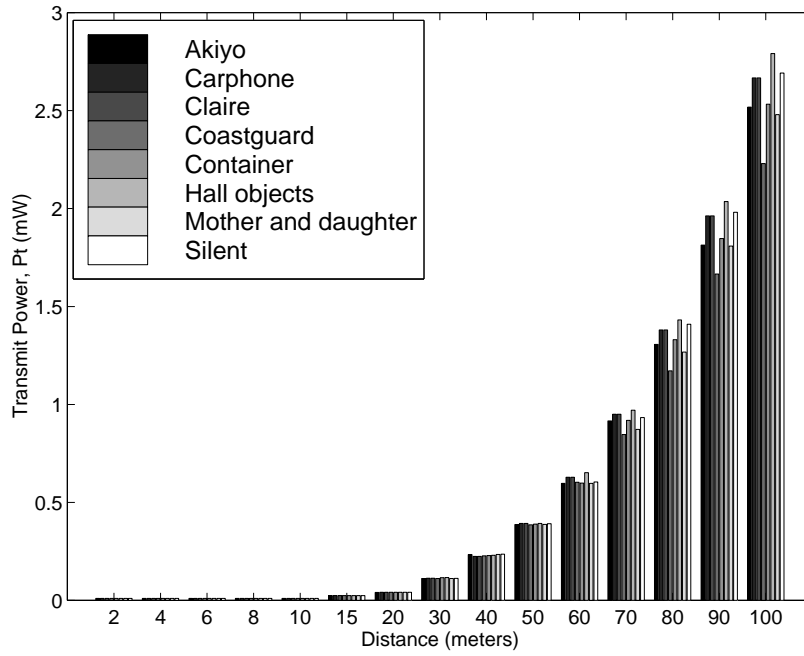


Figure 11: Transmit power consumed in the optimized system.

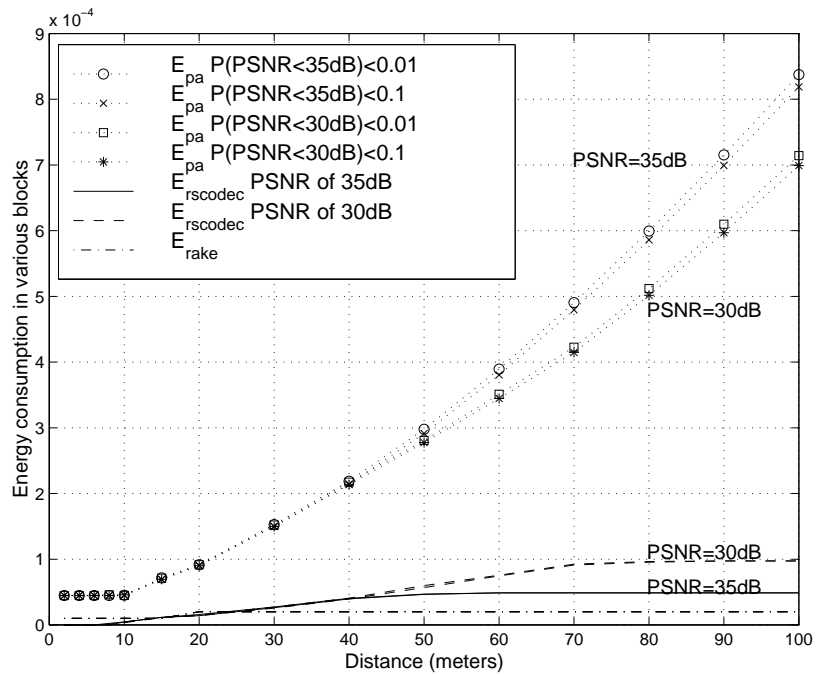


Figure 12: Energy consumed in each component.

the RS codec is smaller than for the PSNR= 30dB constraint at distances over 45m. The higher source rate required to achieve the larger PSNR lowers the channel coding rate. At both PSNRs, the energy consumption of the system achieving the lower $P(\text{fail}) = 0.01$ probability is only slightly larger than the system achieving $P(\text{fail}) = 0.1$ due to the threshold characteristic of the RS coder. The BER of the RS coder as a function of the SNR has a fast transition from $BER = 1$ to $BER = 0$ with only a small change in the SNR.

6 Conclusion

Total-system-energy minimization of a wireless image transmission system is achieved by dynamically reconfiguring the architecture to exploit the variabilities in the image data and the multipath wireless channel. The optimal configuration parameters for the reconfigurable system are chosen to meet performance constraints by trading off the energy consumption of the digital blocks and the power amplifier. Application of the optimization techniques to the indoor office environment shows that the fraction of digital energy consumption to the total energy consumption in the optimized system can range from 29% at a distance of 20m to 14% at 100m. The reduction in total energy consumption in the optimized system averaged (equiprobably) over channels A and B, all distances, both PSNR constraints, and both rates, is 53.6% and 67.3% for a short-range system (under 20m) and long-range system (over 20m), respectively, over a fixed system designed for the worst-case image, distance, and channel. In comparison to a fixed system employing power control to change transmit power, but with fixed digital power, the reduction in total energy consumption drops to 49.4% and 15.6%, respectively, for the short-range and long-range systems. The most significant part of the energy consumption was due to the inefficiency of the power amplifier at short distances. Using a power amplifier with a lower maximum transmit power $P_{t,max} = 50\mu W$ decreased the energy consumption of the system by 60%. Future work on reconfigurable architectures for source coders (especially video coders) and more complex channel coders such as rate-punctured convolutional coders (RCPC) will increase the power consumption of the digital blocks and increase the benefits of a total-system-energy minimization approach.

References

- [1] *Bluetooth Website*. <http://www.bluetooth.com>.

- [2] *HomeRF Website*. <http://www.homerf.org>.
- [3] T. Lan and A. Tewfik, "Adaptive low power multimedia wireless communications," in *1997 Conference on Information Sciences and Systems*, pp. 377–382, 1997.
- [4] J. Rabaey, "Reconfigurable processing : The solution to low-power programmable DSP," in *Proceedings of ICASSP*, (Munich, Germany), pp. 275–278, May 1997.
- [5] M. Goel and N. R. Shanbhag, "Dynamic algorithm transforms for low-power reconfigurable adaptive equalizers," *IEEE Trans. Signal Processing*, vol. 47, pp. 2821–2832, Oct. 1999.
- [6] M. Goel and N. R. Shanbhag, "Dynamic algorithm transformations (DAT) : A systematic approach to low-power reconfigurable signal processing," *IEEE Transactions on VLSI*, vol. 7, pp. 463–476, Dec. 1999.
- [7] S. Appadwedula, D. Jones, K. Ramchandran, and I. Kozintsev, "Joint source channel matching for a wireless communications link," in *International Conference on Communications*, (Atlanta, GA), July 1998.
- [8] J. G. Dunham and R. M. Gray, "Joint source and noisy channel trellis encoding," *IEEE Transactions on Information Theory*, vol. IT-27, pp. 516–519, July 1981.
- [9] A. J. Kurtenbach and P. A. Wintz, "Quantizing for noisy channels," *IEEE Transactions on Communication Technology*, vol. COM-17, pp. 291–302, Apr. 1969.
- [10] V. A. Vaishampayan and N. Farvardin, "Optimal block cosine transform image coding for noisy channels," *IEEE Transactions on Communications*, vol. 38, pp. 327–336, Mar. 1990.
- [11] M. Bystrom and J. W. Modestino, "Combined source-channel coding for transmission of video over a slow-fading Rician channel," in *International Conference on Image Processing*, October 1998.
- [12] V. Chande and N. Farvardin, "Joint source-channel coding for progressive transmission of embedded source coders," in *1999 Data Compression Conference*, (Snowbird, UT), 1999.

- [13] A. Said and W. A. Pearlman, "A new fast and efficient image codec based on set partitioning in hierarchical trees," *IEEE Transactions on Circuits and Systems for Video Technology*, vol. 6, pp. 243–250, June 1996.
- [14] Association of Radio Industries and Businesses (ARIB), *Evaluation Methodology for IMT-2000 Radio Transmission Technologies*, June 1998.
- [15] D. P. Bertsekas, *Nonlinear Programming*. Belmont, MA: Athena Scientific, 1995.
- [16] M. Xakellis and F. Najm, "Statistical estimation of the switching activity in digital circuits," in *Design Automation Conference*, pp. 728–733, June 1994.
- [17] *IBM Website*. <http://www.chips.ibm.com/techlib/products/asics/databooks.html>.
- [18] M. Goel and N. R. Shanbhag, "Low-power channel coding via dynamic reconfiguration," in *Proceeding of ICASSP*, (Phoenix, AZ), pp. 1893–1896, March 1999.
- [19] A. Rofougaran *et al.*, "A single-chip 900-MHz spread spectrum wireless transceiver in 1- μ m CMOS - part I: Architecture and transmitter design," *IEEE Journal of Solid-State Circuits*, vol. 33, pp. 515–534, April 1998.
- [20] L.-J. Lin, A. Ortega, and C.-C. J. Kuo, "Cubic spline approximation of rate and distortion functions for MPEG video," in *Visual Communication and Image Processing*, (Orlando, FL), March 1996.
- [21] R. E. Blahut, *Theory and Practice of Error Control Codes*. Reading, MA: Addison-Wesley, 1983.
- [22] J. G. Proakis, *Digital Communications*. NY: McGraw-Hill, 1989.
- [23] *Image FTP site*. <ftp://sotka.cs.tut.fi/cost/Ossi/sequences/>.
- [24] S. K. Jain, L. Song, and K. K. Parhi, "Efficient semisystolic architectures for finite-field arithmetic," *IEEE Transactions on VLSI*, vol. 6, no. 1, pp. 101–113, 1998.

Appendix A

Derivation of RS Coder Energy Models

In this section, we find the energy consumption models for the Galois field arithmetic modules, RS encoder and decoder.

A.1 GF Arithmetic Modules

Each element in $GF(2^m)$ is defined by a m -bit binary vector. The main Galois field operations are addition, multiplication and inversion. For details on these operations, interested readers are referred to [21].

The addition over $GF(2^m)$ is defined as bit-wise sum of m bits of two operands requiring m XOR gates. It is assumed that standard cells based on $0.18\mu m$, $2.5V$ CMOS technology are being employed. An adder circuit was designed and simulated via the gate-level simulator MED [16]. It was found that the energy consumption per m -bit addition is given by

$$\mathcal{E}_{add} = 3.3 \times 10^{-5} m \text{ (mW/MHz)}. \quad (\text{A.1})$$

For multiplication, a bit-parallel architecture given in [24] was assumed. This architecture requires approximately $2m^2$ XOR gates and $2m^2$ AND gates for each multiplier. It was found by MED simulations [16] that the energy consumption of the $m \times m$ -bit multiplier is given by

$$\mathcal{E}_{mult} = 3.7 \times 10^{-5} m^3 \text{ (mW/MHz)}. \quad (\text{A.2})$$

If \mathbf{a} is a $GF(2^m)$ element, then its inverse is computed as follows:

$$\mathbf{a}^{-1} = \mathbf{a}^{2^m-2} = \mathbf{a}^2 \otimes (\mathbf{a}^2)^2 \otimes \left((\mathbf{a}^2)^2 \right)^2 \otimes \dots \text{ (} m-1 \text{) times}, \quad (\text{A.3})$$

which involves $(2m-3)$ multiplications. Therefore, the energy consumption per m -bit inversion is given by

$$\mathcal{E}_{inv} = 3.7 \times 10^{-5} (2m-3)m^3 \text{ (mW/MHz)}. \quad (\text{A.4})$$

In the following subsections, we employ the energy consumption expressions in (A.1)-(A.4) to derive expressions for the energy consumption of an RS encoder and decoder.

A.2 RS Encoder

A Reed-Solomon (RS) encoder based on the parallel architecture is shown in Fig. 13. We will compute the energy consumption of this encoder. We first explain the operation of this RS encoder. Let $2t$ be the number of check symbols in the n -symbol codeword. Then, in the first $n - 2t$ clock cycles, the information symbols are fed to the encoder, and are simultaneously sent to the output. After $n - 2t$ symbols, the $2t$ latches contain the check symbols, which are then serially shifted to the output codeword. It can be shown that in each of the first $n - 2t$ clock cycles, $2t$ multiply-adds are carried out. Therefore, the energy consumed per codeword generation is given by:

$$\mathcal{E}_{enc/codeword} = 2t(n - 2t)(\mathcal{E}_{mult} + \mathcal{E}_{add}), \quad (\text{A.5})$$

where \mathcal{E}_{add} and \mathcal{E}_{mult} are given by (A.1) and (A.2), respectively.

A.3 RS Decoder

A block diagram of an RS decoder is shown in Fig. 14. The syndrome computation (SC) block computes $2t$ syndromes from the received codeword. These syndromes are then passed to the block implementing the Berlekamp-Massey (BM) algorithm, which generates the error-locator and the error-evaluator polynomials. These polynomials are then processed by the last block, which implements Chien's search algorithm for detecting error locations, and Forney's algorithm for determining the error values. The description of each of these blocks is out of scope of this paper, and the reader is referred to [21] for details and other references. It was found that the energy consumption of these blocks is given by

$$\begin{aligned} \mathcal{E}_{sc} &= 2tn(\mathcal{E}_{mult} + \mathcal{E}_{add}) \\ \mathcal{E}_{bm} &= t^2(10\mathcal{E}_{mult} + 6\mathcal{E}_{add}) + 2t\mathcal{E}_{inv} \\ \mathcal{E}_{cf} &= t(2n(\mathcal{E}_{mult} + \mathcal{E}_{add}) + \mathcal{E}_{inv}) \end{aligned} \quad (\text{A.6})$$

Adding \mathcal{E}_{sc} , \mathcal{E}_{bm} and \mathcal{E}_{cf} in (A.6), we get the energy consumption of the decoder per codeword,

$$\mathcal{E}_{dec/codeword} = (4tn + 10t^2)\mathcal{E}_{mult} + (4tn + 6t^2)\mathcal{E}_{add} + 3t\mathcal{E}_{inv}. \quad (\text{A.7})$$

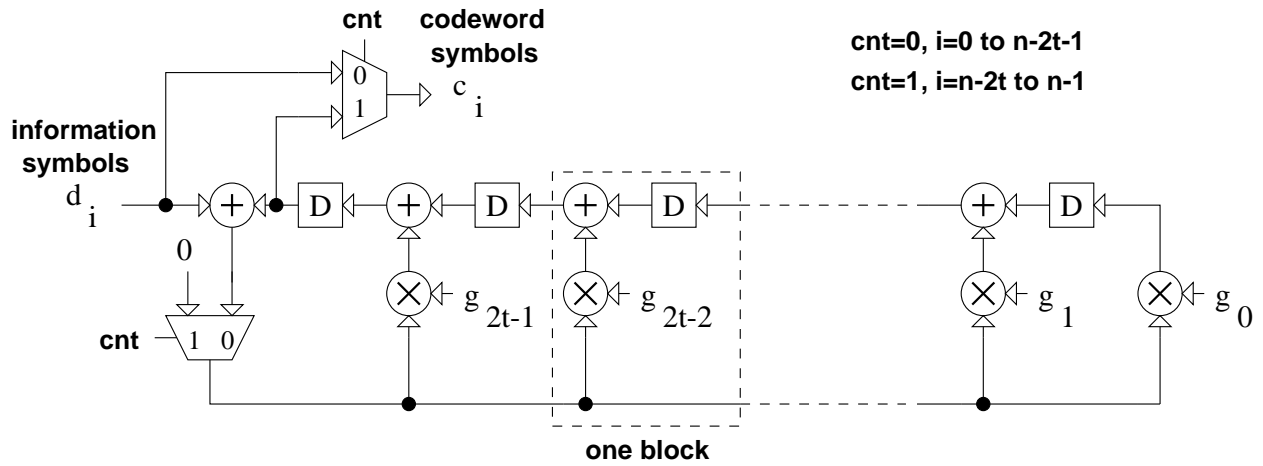


Figure 13: The Reed-Solomon (RS) encoder.

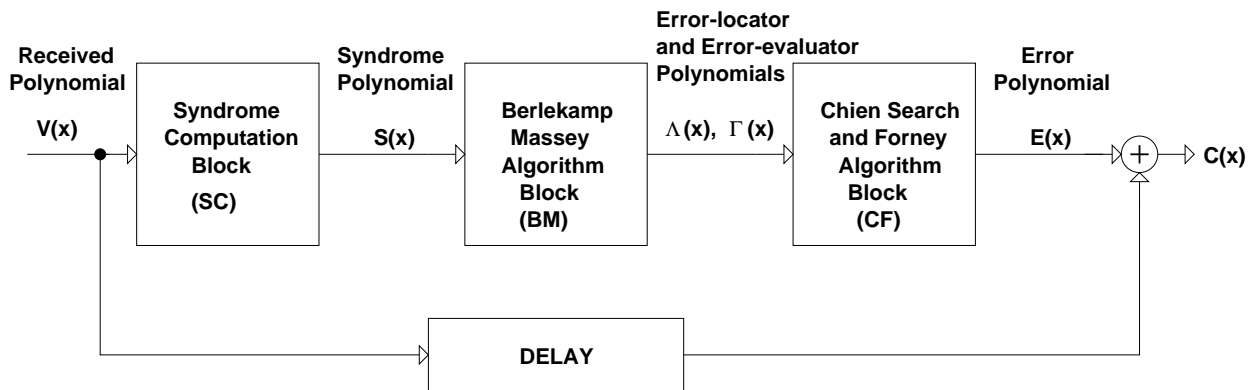


Figure 14: The Reed-Solomon (RS) decoder.

A.4 RS Codec

Energy consumption of the codec can be found by adding the energy consumption of the encoder and the decoder in (A.5) and (A.7), respectively. The energy consumption of the codec per codeword is given by,

$$\mathcal{E}_{codec/codeword} = (6tn + 6t^2)\mathcal{E}_{mult} + (6tn + 2t^2)\mathcal{E}_{add} + 3t\mathcal{E}_{inv}. \quad (\text{A.8})$$

Since $k = n - 2t$ information symbols (each with m bits) are transmitted via each codeword, energy consumption of the codec for processing one information bit is given by

$$\mathcal{E}_{codec/bit} = \frac{\mathcal{E}_{codec}}{m(n - 2t)}. \quad (\text{A.9})$$

Table Captions

1. Configuration space parameters.
2. Indoor office multipath channels [14].
3. System parameters.

Figure Captions

1. (a) Source variabilities (rate-distortion curves) and (b) channel variabilities (bit-error-rate curves).
2. Indoor wireless image transmission system.
3. A reconfigurable multimedia system: (a) the transceiver and (b) the controller.
4. Performance of three configurations m_1 , m_2 and m_3 defined in Table 1.
5. The RAKE receiver: (a) block diagram and (b) architecture of a finger.
6. Comparison between transmit-power-controlled system and optimized system over long range.
7. Comparison between transmit-power-controlled system and optimized system over short range.
8. Comparison between fixed system and optimized system performance.
9. Fraction of energy consumed in each component.
10. Optimized system parameters: (a) protection symbols and (b) RAKE fingers.
11. Transmit power consumed in the optimized system.
12. Energy consumed in each component.
13. The Reed-Solomon (RS) encoder.
14. The Reed-Solomon (RS) decoder.